ACERP: Vol. 2, No. 2, (Spring 2016) 16-21

Advanced Ceramics Progress

Research Article

Journal Homepage: www.acerp.ir

Phlogopite Glass-Ceramic coatings on Stainless Steel Substrate by Plasma Spray

A. Faeghinia*, N. Shahgholi, E. Jabbari

Department of Ceramic, Materials and Energy Research Center, Karaj, Iran

PAPER INFO

Paper history:
Received 30 January 2016
Accepted in revised form 25 July 2016

Keywords:
Fluorophlogopite
Plasma spraying
sub layer
316 stainless steel

ABSTRACT

Granulated glass powder has been plasma sprayed to produce phlogopite (Macor) glass-ceramic coating. Macor glass- ceramic coatings on 316 alloy substrate was prepared by heat treating the resulted glass coated steel. The steel substrate was sand blasted with 35 grid alumina and then bond coated with NiCrAly by plasma spray to provide thermal compatibility between the main coating layer and the substrate. The coating showed chemical stability, and there was no reaction with Fe .The crystallization temperature, thermal expansion coefficient of mica glass-ceramic were 920ºC and 40× 10^{-7}/◦C, respectively. The microhardness of obtained glass-ceramic coating was 6.8GPa and the friction coefficient was 0.98.

1. INTRODUCTION

Glass exists in different forms such as flakes, beads, microspheres, fibers, and powder. Glass flakes provide the best coating barrier properties. Other forms of the glass can also form a protective barrier because of their close packing in the coating. Glass is used in when high temperature resistance or high resistance to abrasion, erosion and impact is needed. Glass coating is usually preferred for elevated temperatures, not only because of its ability to maintain chemical resistance at high temperatures but also because of its coefficient of thermal expansion.

Glass flake can obtain thermal expansion properties close to those of carbon steel. This enables them to retain good adhesion even under thermal shock [1].

Glasses are extremely versatile materials, easy to process, and capable of producing high-quality surface finishes. Glass also provides effective coatings in many applications owing primarily to its dense structure, corrosion resistance, aesthetic appearance and low cost. Enamels are impossible to scratch and products of any shape and color can be enameled such as baths, washing machines, gas and electric cookers, hot water services, storage tanks, car exhaust systems, street signs, interior and exterior architectural panels, fascia and partitions [2].

*Corresponding Author's Email: Aida.faeghinia@gmail.com (A. Faeghinia)

Phlogopite is chemically an aluminosilicate occurring in large amounts in natural deposits and is more easily available than specularite. Phlogopite has comparable advantages to pigments including lower specific density (2.9 g. cm^{-3}) and thus a lower tendency to sedimentation in a liquid medium. Published papers indicated the anticorrosion barrier efficiency of this mineral as pigments [3].

The diameter –to- thickness ratio of this group exceeds 25:1, higher than that of any other flaky pigment. This makes mica very effective at building up layers of pigment in the dried film, thus increasing the pathway that water must travel to reach the metal and reducing water permeability [4].

For these reasons, we tried to use the advantages of both glass and Phlogopite phases in mica glass –ceramic as an anticorrosion coating. Different coating techniques have been introduced such as dip coating, electrophoretic deposition, sintering, hot isostatic pressing, flame spraying and plasma spraying [5].

Plasma spraying is most popular deposition technique due to its process feasibility as well as reasonably high coating bond strength and mechanical property [6]. Several bioactive materials, such as hydroxyapatite (HA) [7] and bio glass (BG) [8] have been coated onto metals and alloys substrates by plasma spraying. The object of this work was to deposit Macor on 316 alloy substrate by atmospheric plasma spraying (APS) and to investigate microstructure, phase composition, wear and chemical resistance of the coatings.

2. EXPERIMENTAL DETAILS

The glass composition was prepared according to Table 1. The raw materials of glass were K_2CO_3 (Merck Art No. 7734), $MgCO_3$ (MERCK art. no. 5828), Al_2O_3 (Merck Art 5550), MgF_2 (7783-40-6), TiO_2 and pure optical grade silica, melted in an electric furnace in a platinum crucible at the temperature range of 1400 to 1450°C for 1–2 hr.

The resulting melt was quenched in cold distilled water. The obtained frit was ground in an agate mortar then sieved to give fine (<45μm) frits. The frites were mixed by 7%PVA, aged for 24 hr. and then passed through a No.40 screen to reach the granulated frit, which is necessary for high spray ability.

The fine frit was used for subsequent use in DTA analysis. DTA analysis (Netzsch320) which was utilized to determine the crystallization temperature of glass, was performed using 6mg of glass powders in an alumina crucible in air at a heating rate of 10 ◦C/min.

TABLE 1. The nominal composition of studied glass in wt.%

	SiO_2	Al_2O_3	B_2O_3	K_2O	MgO	TiO_2	F-
Wt.%	35	14	12	6	21	5	14

In order to improve the microstructure and the mechanical properties of the as-sprayed Macor coatings by sintering and crystallization, thermal treatments were performed in an electric furnace. The heating rate was 10 °C/min. On the basis of the glass transition and crystallization temperatures obtained from STA analysis, pre-sintering isotherms were chosen in order to obtain sintered coatings with a good microstructure. Heat treating isotherms at 650 °C for 1 h were performed on Macor frites. Figure 1. shows the XRD pattern of obtained frites. The recorded XRD patterns of the as-received frites confirm the amorphous nature of the glass powder: only very broad intensity humps in a range of 2θ~40°-60° was observed for the glass powder before deposition on the substrate but after the spraying and heat treating the glass coating it crystallized.

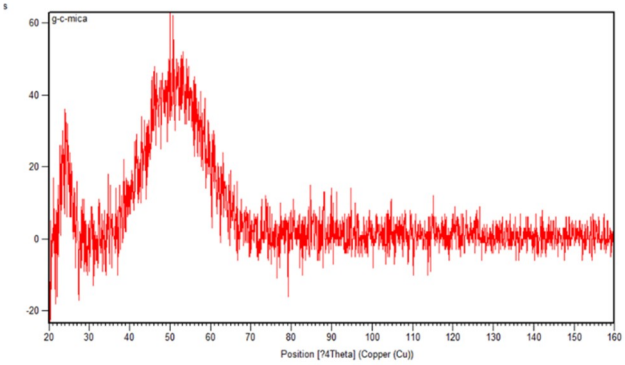

Figure 1. shows the amorphous nature of obtained frites by XRD.

A plasma torch consists of a tungsten cathode, water cooled copper anode with a central nozzle, and a gas feeding system was used. An arc is struck between the cathode and the anode across the gas flux, so that ionization of atoms and molecules transforms the gas into a hot (up to 5,000 K) and high-velocity plasma. The coating material, in powder, is radially fed into the plasma flux just outside the nozzle exits: the particles are therefore dragged and heated by the plasma itself, so that they melt and accelerate towards the substrate. The melted droplets impact on the substrate, flattening and solidifying in a few microseconds, assuming a typical lamellar (or splat-like) morphology. Every splat develops high tensile stresses after solidification because of its rapid cooling. In brittle materials, these stresses can only be relaxed through cracking: therefore, the coating is quite defective because of intraplate and inter plate micro cracks, and also because of some pores; hence, several sealing procedures have been developed [14].

The glass powders were plasma-sprayed on 316 alloy substrates using a system equipped with a 3MB torch, in APS mode, using the operating parameters listed in Table 2.

However, the deposition mechanism is not fully understood, and in particular the effect of the glass composition has not been clarified. The high thermal energy of the plasma jet (Argon - based) can cause thermal shock in the deposited glass during the spraying. Moreover, plasma spraying may generate partially molten large glass particles and decomposed fine particles, and these can increase the flaws (porosity and micro cracks) in coatings. Moreover, the high melt viscosity of the glass prevents the splats from flattening on the steel substrate and reduces adhesion of coatings. The un melted particles can also affect coating microstructure by increasing pores in coatings and this can affect the properties of coatings [7].

The substrates of 316 alloy, having dimensions of 15mm×10mm×2mm, were grit blasted with SiC particles before deposition. After being ultrasonically washed in acetone and rinsed in deionized water, the surface of sample was coated by NiCrAly as a sub layer directly by Macor glass (To provide thermal compatibility between main coating layer and substrate) [16].

After that, the sample was heat treated at 620-916ºC in order to reach the dense Phlogopite glass-ceramic.

TABLE 2. Plasma torch operating parameters.

Operating parameters	Spraying distance [mm]	Feed rate [gr/min]	Current [A]	Ar/H_2 flow	Nozzle diameter [mm]
Macor coating	100	15	400	85/15	6.5

The surface of samples was sputter coated with gold for morphological observation or with carbon for elemental analysis. The phase analysis of coatings was performed by using an X-ray diffractometer (XRD: Siemens,

Germany), operating with Cu Kα radiation at 30 kV and 25 mA. The analyzed range of the diffraction angle (2θ) was between 20° and 70°, with a step width of 0.02°.
The Vickers hardness of the heat treated coating was measured under an indentation load of 50 g for 20 s. In order to obtain reliable statistical data, analysis points were spaced so as to eliminate the effect of neighboring indentations, and the hardness was evaluated by taking five indentations on each specimen and averaging of only three middle values (S) [4]. The hardness of the as-sprayed plasma sprayed sample was 4.7 GPa (S=0.32) and after heat treating at 800°C for 1 hour this increased to 6.8 GPa (S=0.76).
Pin-on-disc is the most widely used wear test, followed by pin-on-flat. Other applications of pin-on-disc include material wear and friction properties at elevated temperatures and in controlled atmospheres [8]. Almond et al. [9] used a pin-on-disc apparatus for testing ceramics and cemented carbides on alumina discs using the pin as the test material. In a two-body abrasion test, a coated pin is pressed against a rotating abrasive paper making a spiral path to avoid overlapping [10]. This test process is very common for thin coatings using a diamond tip as the abrading tool.
This test was performed on heat treated plasma deposited coatings. Wear tests were performed in accord with the ASTM G99 for wear testing with a pin-disk apparatus. The wear rate of the materials was determined at a load of 1.50, 1.20, 0.9, 0.3 kgf, rotating speed of 0.1m/sec, sliding distance of 30m using a pin-on-disk tribometer.

3. RESULT AND DISCUSSION

Figure 2 and 3. represent the results of DTA and dilatometer of the resulted Macor glass. The DTA trace shows T_g (glass transition temperature) and three T_p (crystallization temperatures) at 620°C and 800°C, 850°C, 916 °C, respectively. Dilatometer shows softening temperature at 677ºC. The samples were heat treated at two steps, i.e. at $T_g+T_d/2$=620ºC and then at 800, 850 (the temperatures prior and after the DTA exothermic peak 820ºC), 916ºC (second peak), respectively.

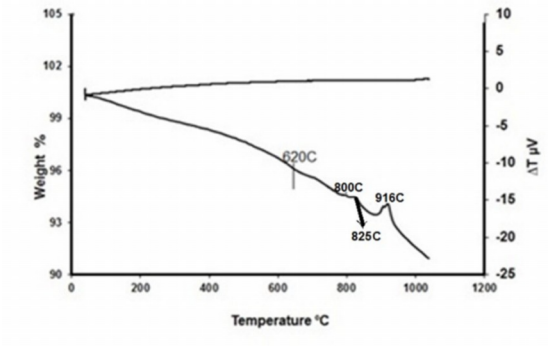

Figure 2. The DTA result of Macor glass frits.

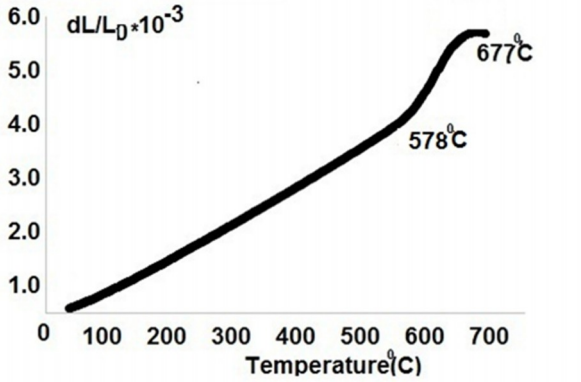

Figure 3. Thermal expansion coefficient of Macor glass.

Figure 4. shows the XRD results of samples heat-treated at DTA peaks. According to Figure 2. the crystallization of MgF_2 occurs at 800º C and the phlogopite phases were appeared at 850ºC as proved by subsequent X-ray analysis in Figure 4. The fluorine loss of glass composition has been reported in previous articles [11,12,13] which can result in magnesium and silicon rich phases corresponding to forsterite formation at 916ºC. [2]. The crystallization mechanism of this glass ceramic has been studied in other papers. But it seems that (responding to others proven work) the exothermic peak at 916ºC can be related to forsterite formation.
It is well known that interfacial microstructures reveal visible information about the bonding mechanism and joint properties. Figure 5. shows SEM micrographs of the cross section of the as-sprayed Macor glass ceramic coatings. Stainless steel is bonded to a glass–ceramics, and emphasis was placed on clarifying the interfacial microstructure of the joint metal/glass–ceramics through a scanning electron microscope (SEM) and an energy dispersive X-ray spectroscopy (EDS) in this study.

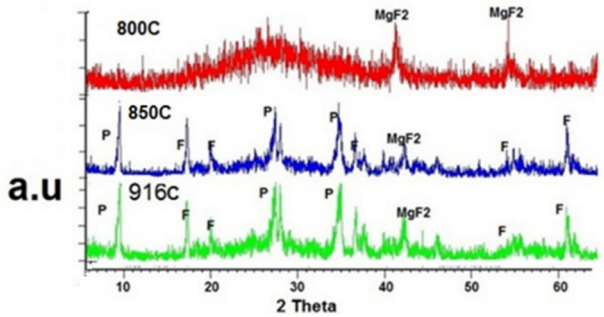

Figure 4. XRD results of heat treated glass at 800,850,916ºC.

Typical fracture morphology of the tested presents the interfacial images of the profile section of the joint. The SEM pictures of Figure 5A. show the NiCrAly elements with 135 micrometers in size between the stainless steel/glass–ceramics interface. Figure 5B. presents the glass–ceramics side contains the elemental of magnesium, oxygen, fluorine, aluminum, silicon, k and Ti according to the EDS results. The EDS results in

Figure 5C. suggest that the porosities on NiCrAly side contain Fe and Si which come from stainless steel. Figure 5D. and 5E show the oxygen ions and NiCrAlY elements which were congregated in the bonding interface in the dark holes and grey part between glass and NiCrAly. Also, it can be seen that the coating is characterized by a rough surface, with some partially melted particles Figure 5A. Under higher magnification, the structure of the coating appears to be highly melted and few micro-cracks on the surface of the coating Figure 5A. The cracks can be related to the mismatching of thermal expansions of the coating and the metal, which should be minimized to avoid excessive stress generation at the interface [14].

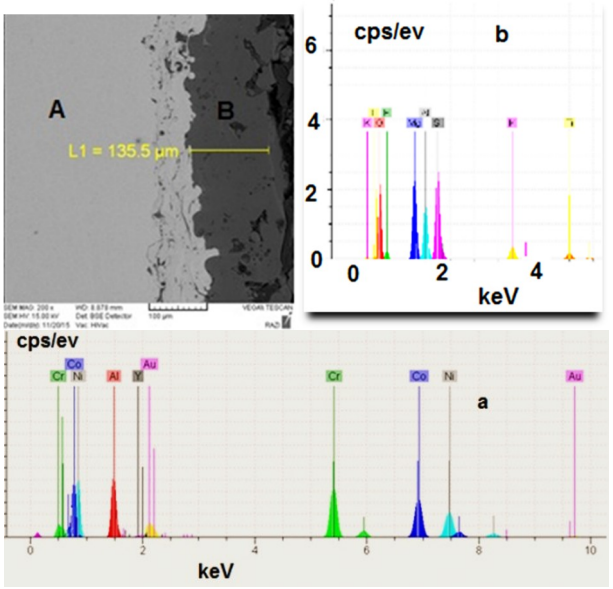

Figure 5. (a) The SEM micrographs of surfaces show the NiCrAly of 135 micrometers in size between the stainless steel/glass–ceramics (b)The glass-ceramic side of coating.

The metallographic study of the interface boundary established that during firing as a result of the heterogeneous interaction on the "steel–enamel" contact surface and di□usion processes, there is a transitive inter phase approximately 2µm thick (point e) which shows the Si and Mg diffusions from glass through the NiCrAly. The microstructures show globular pores, inter lamellar pores along with cracks. High magnification images (Figure 5cand d) show the detailed coating buildup and the Oxygen diffusion through the NiCrAly, resulted in porosity formation. The microstructure shows the extended structure within the individual splats indicative of complete melting.

3.1. Wear resistance results

The profile curve of the wear groove of the sprayed sample using the steel pin can be seen in Figures 6a-c. The friction coefficient was continuously recorded during the sliding test.

Static friction is the force required to initiate sliding (Figure 6a first stage). The existence of this force suggests that the two surfaces are interlocked into a local free energy minimum. The friction force is the lateral force required to lift the surfaces out of the local minimum.

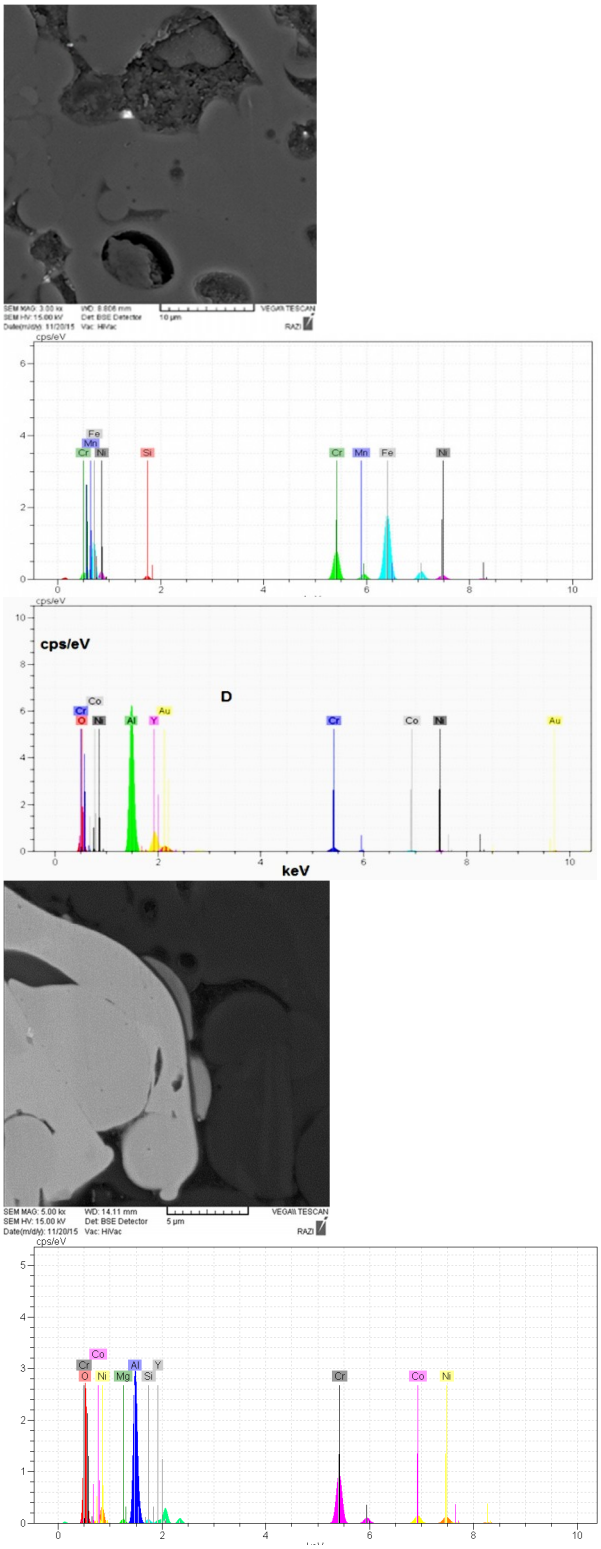

Figure 5. (c) The inside of NiCrAly side porosities analysis (d) the interface of NiCrAly and glass-ceramic analysis (e) the intermediate phase formed on the glass particles.

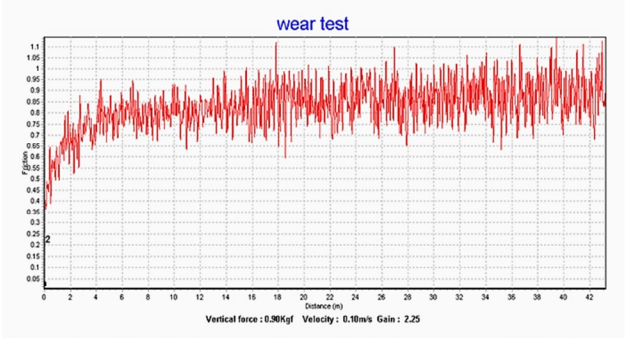

Figure 6a. The friction coefficient V.S distance by 0.90kgf

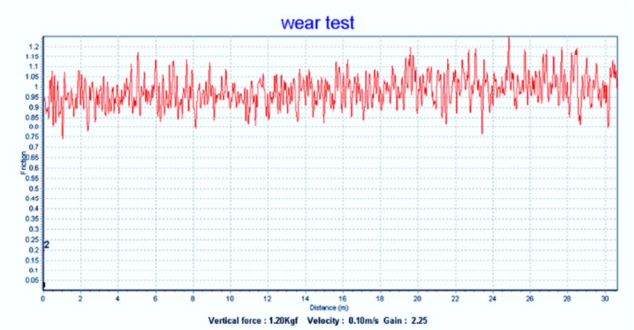

Figure 6b. The friction coefficient V.S distance by 1.20kgf

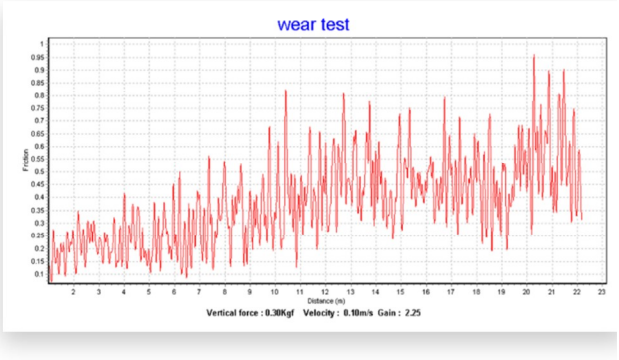

Figure 6c. The friction coefficient V.S distance by 0.10kgf .

As a sliding surface moves across the stationary surface, the kinetic energy of the sliding surface is transferred to the stationary surface, causing a temperature increase (Figure 6b). This increase can alter the face of the stationary surface, affecting the rate at which friction increases with load. At high load, the transfer of heat could become faster, effect on the friction. When this occurs, the friction deviates from linearity. There is no reason why the peaks and troughs in surface free energy between surfaces should be correlated (except in the exceedingly rare case of lattice commensurability). One expects that at any moment of time, some peaks are moving up a ramp while others are moving down (Figure 6c). An initial period of rapid wear was followed by a more gradual wear stage. Or it can be said that, the rapid wear is due to the running-in of the two sliding surfaces involving the removal of protrusions, high spots, and misalignments due to the high local stresses. As sliding progresses, the contact stresses reduce, and the wear mode transforms into the milder equilibrium stage. Owing to the inevitable minor variations in setting up the test and in the sample surface finish, the equilibrium wear stage is more reproducible, and this was used as the indicator of the wear of the coatings.

Influence of the load on wear

The weight loss was found to increase with increasing distance (Figure 7.) This is due to the influence of the material microstructure on the wear mechanisms. Furthermore, as the wear test progresses, the initial damage mechanisms affect the subsequent material behavior.

The sliding action modifies the stress field and, in particular, introduces a significant tensile component immediately behind the moving slider. This combines with the biaxial-tensile residual stress already present (as a result of thermal stresses generated during deposition) to initiate cracks normal to the sliding surface and to create the cracks resulted in the more weight loss.

Crack formation leads to material removal and debris formation. The debris particles act as abrasive particles leading to further wear, thus complicating the entire material response.

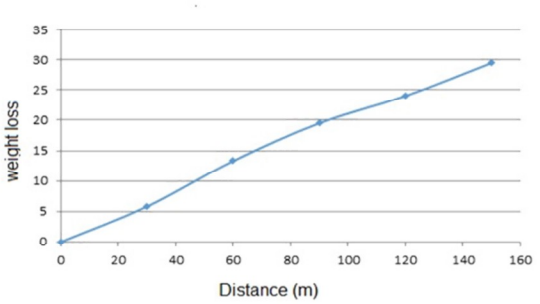

Figure 7. The weight loss V.S distance (m)

3.2. Corrosion properties

The chemical resistance was measured in the devitrified glass-ceramic steel coatings. The glass-ceramic coated sample was boiled in 10wt% HCl for 7 days. No obvious weight loss was detected in this sample. According to the calculations, the obtained silicate–enamel coating reduces the corrosion rate of steel by 3–4 orders of magnitude. In complex silicate glasses, the cavities and pores of coated surface are occupied by metal ions, which prevent the penetration of oxygen through these glasses (Figure 5.) By plasma spray processing, the penetration of oxygen through a Macor glass-ceramic coating proceeds via macro- and micro-pores, involving metal ions which increase the protective effect.

4. CONCLUSION

Due to the high hardness, the amorphous coatings show good wear characteristics. The friction coefficient was

0.95 under 0.90 kgf with 0.1m/s velocity in the body abrasion tests in the heat treated plasma sprayed Macor coatings. However, the body abrasion resistance of the heat treated glass-ceramic was not as good as the commercially mature WC-cemented carbide coatings. These results can be interpreted based on the hardness of the substrates. The Macor glass-ceramic coating has the (6.8 GPa) and exhibited good chemical resistance. Generally, when the ratio of the hardness of the abrasive divided by the hardness of the substrate approaches or exceeds unity then the abrasive wear resistance increases significantly.

REFERENCES

1. Someswar, D., "A new high temperature resistant glass–ceramic coating for gas turbine engine components", ***Bulletin Material Science,*** Vol. 28, No. 7,(2005), 689–696.
2. Conde, A. and Damborene, J.,"Monitoring of vitreous enamel degradation by electrochemical noise", ***Journal of Surface and Coatings Technology***, Vol. 150, (2002), 212–217.
3. Minghui, C. and Wenbo, L., "Glass coatings on stainless steels for high-temperature oxidation protection: Mechanisms", ***Corrosion Scienc,*** Vol. 82, (2014), 316–327.
4. Mukhopadhyay, A. K., Datta, S. and Das, G.C., "Hard glass-ceramic coating by microwave processing", ***Journal of the European Ceramic Society***, Vol. 28 ,(2008), 729–738.
5. Min'ko, N.I. and Matveeva, T.A,, "Glass Enamels For Steel and Cast Iron articles(Review)", ***Glass and Ceramics,*** Vol. 56, No.11, (1999), 12-16.
6. Datta, S., "Application of design of experiment on electrophoretic deposition of glass-ceramic coating materials from an aqueous bath", ***Bulletin Material Science,*** Vol. 23, No. 2, (2000), 125–129.
7. Hasso, F., "Glass Coatings By Combustion Flame Spraying: the Microstructure and Properties", ***Universal Journal of Materials Science***, Vol. 1, No. 3, (2013), 149-158.
8. Almond, E.A., Lay, L.A. and Gee, M.G., "Comparison of sliding and abra sive wear mechanisms in ceramics and cemented carbides", ***Institute of Physics Conference Series,*** No. 75, (1986), 919 – 948.
9. Bouslykhane, K., Moine Villain, J.P. and Grilhe, J." Mechanical properties and wear resistance of ion-beam assisted sputter-de-posited NiTi(N) coatings", ***Surface and Coatings Technology,*** Vol. 49, (1991), 457 – 461.
10. Baik, D. S., "Crystallization of fluoreckermannite in glass", ***journal of materials science letters***, Vol. 15, (1996), 558- 560.
11. Beall, G. H., "Design and Properties of Glass-Ceramics", ***Annual Review of Materials Science***, Vol. 22, (1992), 91-119.
12. Wood, D. and Bubb, N., "Investigation into the crystallization of Dicor glass-ceramic", ***Journal of Materials Science Letters,*** Vol. 18, No. 13, (1999), 1001-1002.
13. Bolellia, G. and Cannilloa, V., "Plasma-sprayed glass-ceramic coatings on ceramic tiles: microstructure, chemical resistance and mechanical properties", ***Journal of the European Ceramic Society,*** Vol. 25, No. 11, (2005), 1835-1853.
14. Meigin, S., Fujimasa, M., "The Friction and Wear Properties of PTFE Composite-Thermal Spray Metallic Binary Coatings", ***Materials Transactions,*** Vol. 46, No. 1, (2005), 84 - 87.
15. Gawne, D.T., Qiu, Z., Bao, Y., Zhang, T. and Zhang, K., "Abrasive Wear Resistance of Plasma-Sprayed Glass-Composite Coatings", ***Journal of Thermal Spray Technology***, Vol. 10, No. 4, (2001), 599 -604.